nature physics

Article

https://doi.org/10.1038/s41567-025-02874-0

Observation of polarization density waves in $SrTiO_3$

Received: 29 April 2024

Accepted: 10 March 2025

Gal Orenstein[1,2,16], Viktor Krapivin[1,2,3,16], Yijing Huang[4], Zhuquan Zhang[5], Gilberto de la Peña Muñoz[1,2], Ryan A. Duncan[1,2], Quynh Nguyen[1,2], Jade Stanton[3,6], Samuel Teitelbaum[6], Hasan Yavas[7], Takahiro Sato[7], Matthias C. Hoffmann[7], Patrick Kramer[7], Jiahao Zhang[8], Andrea Cavalleri[9], Riccardo Comin[10], Mark P. M. Dean[11], Ankit S. Disa[12], Michael Först[9], Steven L. Johnson[13,14], Matteo Mitrano[15], Andrew M. Rappe[8], David Reis[1,2,3], Diling Zhu[7], Keith A. Nelson[5] & Mariano Trigo[1,2] ✉

The nature of the incipient ferroelectric transition in $SrTiO_3$ has been a long-standing puzzle in condensed matter physics. One explanation involves the competition between ferroelectricity and an instability characterized by the mesoscopic modulation of the polarization. These polarization density waves, which should intensify near the quantum critical point, break local inversion symmetry and are difficult to characterize with conventional X-ray scattering methods. Here we probe inversion symmetry breaking at finite momenta and visualize the instability of the polarization at the nanometre scale in $SrTiO_3$ by combining a femtosecond X-ray free-electron laser with terahertz coherent control methods. We found polar-acoustic collective modes that are soft, particularly at the tens of nanometre scale. These precursor collective excitations provide evidence for the conjectured mesoscopic-modulated phase in $SrTiO_3$.

$SrTiO_3$ exhibits characteristics typical of an incipient ferroelectric (FE) material, such as an increase in the dielectric constant[1] and polar-mode softening[2] upon cooling. However, quantum fluctuations at low temperatures prevent long-range polar order in this material, rendering it a quintessential example of a quantum paraelectric material[3]. Nevertheless, $SrTiO_3$ exhibits mesoscopic fluctuations of the FE polarization and develops polar nanoregions at low temperatures, which have a substantial impact on the properties of the material[4–7]. An FE phase in $SrTiO_3$ can readily be obtained by various methods such as strain[8,9], calcium substitution[10] or oxygen isotope substitution[11]. More recently, experimental and theoretical studies have shown that FE features can be induced by driving vibrational modes using ultrafast terahertz and mid-infrared (IR) pulses[12–15]. These properties of $SrTiO_3$ indicate its close proximity to an FE instability at low temperatures.

The FE instability is well established and is associated with the softening of an optical polar mode at zero wavevector. However, several susceptibility and neutron-scattering measurements have led to speculation that fluctuating polar-acoustic modes with finite wavevectors

---

[1] Stanford PULSE Institute, SLAC National Accelerator Laboratory, Menlo Park, CA, USA. [2] Stanford Institute for Materials and Energy Sciences, SLAC National Accelerator Laboratory, Menlo Park, CA, USA. [3] Department of Applied Physics, Stanford University, Stanford, CA, USA. [4] Department of Physics, University of Illinois at Urbana-Champaign, Urbana, IL, USA. [5] Department of Chemistry, Massachusetts Institute of Technology, Cambridge, MA, USA. [6] Department of Physics, Arizona State University, Tempe, AZ, USA. [7] Linac Coherent Light Source, SLAC National Accelerator Laboratory, Menlo Park, CA, USA. [8] Department of Materials Science and Engineering, University of Pennsylvania, Philadelphia, PA, USA. [9] Max Planck Institute for the Structure and Dynamics of Matter, Hamburg, Germany. [10] Department of Physics, Massachusetts Institute of Technology, Cambridge, MA, USA. [11] Condensed Matter Physics and Materials Science Department, Brookhaven National Laboratory, Upton, NY, USA. [12] School of Applied & Engineering Physics, Cornell University, Ithaca, NY, USA. [13] Institute for Quantum Electronics, Physics Department, ETH Zurich, Zurich, Switzerland. [14] SwissFEL, Paul Scherrer Institut, Villigen PSI, Switzerland. [15] Department of Physics, Harvard University, Cambridge, MA, USA. [16] These authors contributed equally: Gal Orenstein, Viktor Krapivin. ✉e-mail: mtrigo@slac.stanford.edu

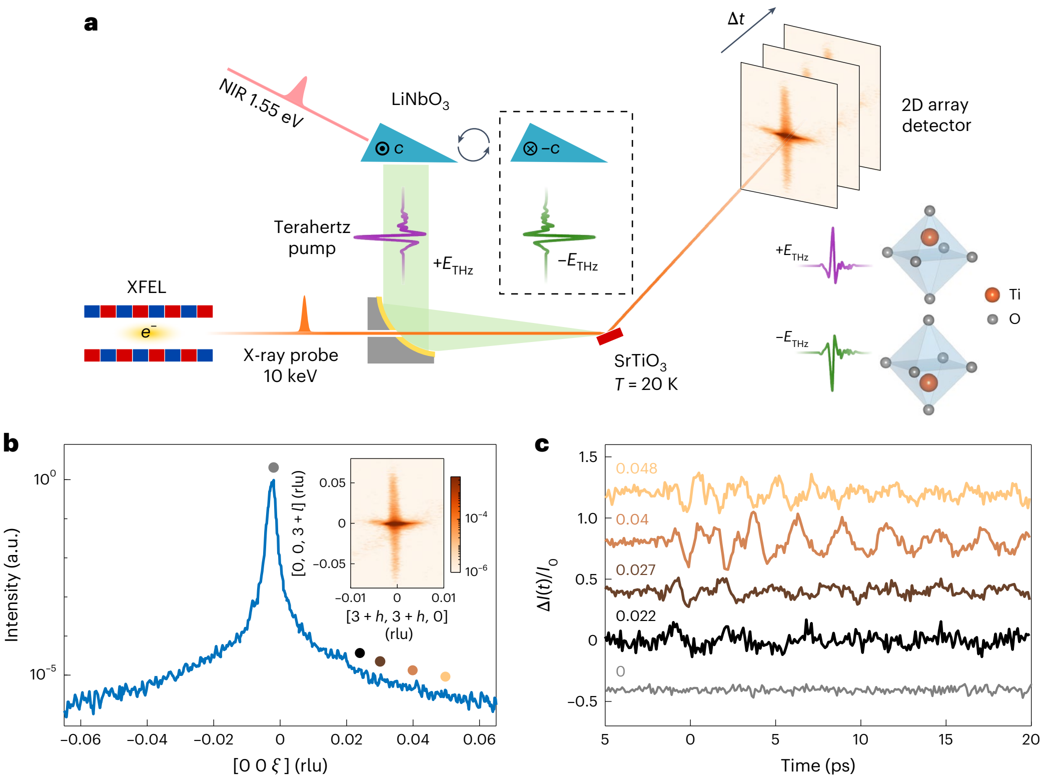

Fig. 1 | Ultrafast hard X-ray scattering under strong terahertz excitation. **a**, Left: schematic illustration of the experimental set-up. Pulses with a spectrum centred at 0.5 THz (Supplementary Fig. 1) and electric field waveform denoted by E_{THz} were produced by optical rectification of 100-fs NIR pulses centred at 800 nm. Two LiNbO$_3$ crystals with FE polarizations pointing in opposite directions enabled the polarity of the emitted radiation to be swapped by vertically translating the LiNbO$_3$ prisms into the incident NIR beam. The terahertz pulse was focused onto the SrTiO$_3$ sample using a parabolic mirror. This pulse was collinear with the X-ray probe pulse and had a photon energy of 10 keV. Right: illustration of the polar displacement of the Ti atom upon excitation with fields of opposite polarity. **b**, Integrated intensity around the (3, 3, 3) Bragg peak, as a function of ξ, in the [3, 3, 3+ξ] direction at a temperature T = 20 K. Inset: X-ray scattering intensity in a section of reciprocal space around the (3, 3, 3) peak, as a function of h and l, in the [3+h, 3+h, 3+l] plane. **c**, Relative change in intensity (Δ$I(t)/I_0$) for representative wavevectors along the [001] direction indicated by the colour-coded dots in **b**. The wavevectors are labelled next to each trace. 2D, two dimensional; XFEL, X-ray free-electron laser.

strongly affect the quantum paraelectric regime at low temperature[16–20]. These results may indicate the existence of another structural instability in SrTiO$_3$ that is different from the homogeneous FE state, with strong lattice fluctuations on the nanometre scale, potentially heralding a new phase with spatially modulated polarization[16,19,21]. However, the crucial element of this putative polar-acoustic regime—the mesoscopic polar characteristics of SrTiO$_3$—could not be determined by these measurements and had to be indirectly inferred from models.

Here we probe the mesoscopic polar dynamics of SrTiO$_3$ at femtosecond timescales using ultrafast hard X-ray diffraction and diffuse scattering[22] at the Linac Coherent Light Source[23]. Ultrafast hard X-ray scattering allowed us to resolve the polar dynamics as a function of the wavevector and to unravel the evolution at nanometre scales. By contrast, optical second harmonic generation, which has been used in several previous studies[12–14], is a highly sensitive measurement of the polar excitation. However, it typically probes only the near-zero wavevector response. To induce the transient states[12], we used single-cycle pulses of terahertz radiation resonant with the soft modes of SrTiO$_3$, as illustrated in Fig. 1a (see Methods for details). Previous femtosecond X-ray diffraction measurements have directly revealed the atomic displacements driven by terahertz pulses in SrTiO$_3$ thin films[24]. We developed an approach for probing inversion symmetry breaking to explore the enigmatic low-temperature quantum paraelectric regime in bulk single crystals. To characterize the polar properties of the transient lattice distortions, we devised a scheme for switching reproducibly between opposite polarities of the generated terahertz field. Related methods have demonstrated the ability to manipulate ferroic orders[25]. In this work, we show that when combined with diffuse X-ray scattering, this method is an incisive probe of polar modes and inversion symmetry breaking (Fig. 1a) at the nanoscale.

Figure 1b shows the equilibrium X-ray intensity around the (3, 3, 3) Bragg peak along the [001] direction (pseudo-cubic notation), at a temperature of T = 20 K. Below T = 105 K, SrTiO$_3$ adopts a tetragonal structure whose twin domains can be identified in the scattering[26–29] (Supplementary Fig. 2). We focused on domains that have their c axis oriented in the direction of the sample normal, [001]. The reciprocal space map in the inset of Fig. 1b shows that the intensity is characterized by strong directional scattering along the sample normal, which represents heterogeneity in the lattice mostly in the [001] direction.

Figure 1c shows the differential X-ray intensity Δ$I(t)/I_0$ as a function of the pump–probe delay at different representative wavevectors along the [001] direction, where Δ$I(t) = I(t) - I_0$ and I_0 is the X-ray intensity before the terahertz excitation. Most of the signal was localized in the range ξ = 0.03 to 0.06 reciprocal lattice units (rlu) (Fig. 1b), corresponding to length scales of 10–20 nm, whereas the ξ = 0 signal at the Bragg peak (grey line) did not show an appreciable dynamic response. This was surprising, as the strongest resonance to the spatially uniform incident field was expected to be from the transverse optical (TO) mode at ξ = 0 (ref. 12). The lack of signal at long wavelengths (grey line) means that we did not observe a strong uniform response of the system as a whole. Furthermore, momentum conservation forbids direct terahertz excitation at high wavevectors in a homogeneous sample. Thus, these signals arose from inhomogeneous excitation by the pump, which can occur only through pre-existing inhomogeneities in the sample. The 10–20-nm

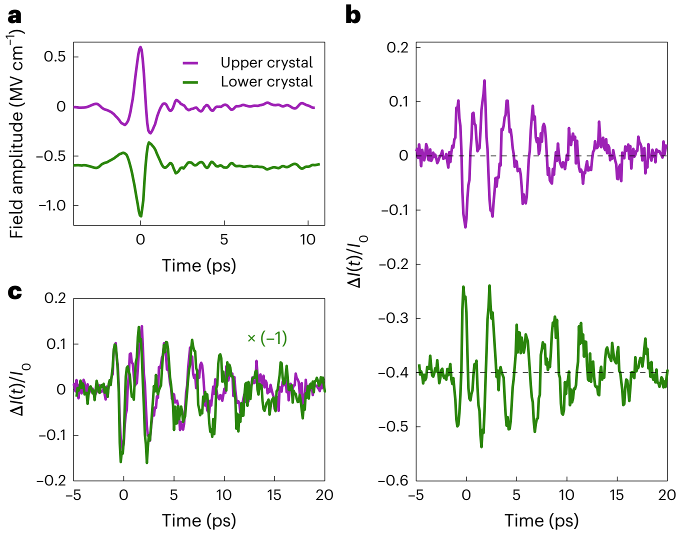

Fig. 2 | Odd symmetry of the ultrafast response. a, Electro-optic sampling measurement of the terahertz pulse profile. The purple (green) trace represents the terahertz pulse generated by the upper (lower) $LiNbO_3$ crystal. The effect of internal reflection inside the electro-optic sampling crystal was removed by a standard procedure[39]. **b**, Dynamics of $\Delta I/I_0$ following terahertz excitation at a temperature of $T = 20$ K, integrated between 0.03 and 0.04 rlu. The purple and green traces represent the response following the terahertz pulse generated by the upper and lower $LiNbO_3$ crystals, respectively. **c**, Same as **b** but with the signal for the lower crystal inverted.

length scale was not determined directly by the non-uniformity of the propagating terahertz beam, as the attenuation length of the terahertz radiation was of the order of 500 nm and the lateral profile has a ~1 mm diameter (see Methods for details). Furthermore, the spectrum of the pulse extended at most to 3 THz (Supplementary Fig. 1), which corresponds to a wavelength of $\lambda_{\mathrm{min}} \approx 100$ µm, so non-uniformity was diffraction limited to $\lambda_{\mathrm{min}}/2 \approx 50$ µm. As we discuss below, the 10–20-nm length scale coincides with wavevectors at which the transverse acoustic (TA) and TO modes are most strongly coupled[17,20,30].

To characterize these terahertz-induced excitations, we devised a scheme to invert the polarity of the generated terahertz field by switching between two $LiNbO_3$ prisms mounted with their FE polarizations pointing in opposite directions, as shown in Fig. 1a. Figure 2a shows the electro-optic sampling traces of the two terahertz pulses generated by this set-up. The pulses are inverted and otherwise nearly identical. Figure 2b shows $\Delta I(t)/I_0$ following excitation by the two terahertz waveforms and integrated over wavevectors $\xi = 0.03$ to 0.04 rlu, using the same colours as Fig. 2a to reference the corresponding field polarity. For better comparison, Fig. 2c presents the same data with one of the traces flipped, which shows that $\Delta I(t)$ was inverted when the terahertz field was inverted, directly revealing that these oscillations originated from polar collective modes. These polar modes break both local inversion and translational symmetry (conservation of crystal momentum) as they evolve on their natural timescales, and they enable direct dipole coupling to the long-wavelength terahertz radiation. We associated this inhomogeneity with polar nanoregions, which play an important role in the quantum paraelectric phase of $SrTiO_3$ (refs. 4–6).

Further insight into the nature of these excitations was gained by identifying how the different frequency components of the oscillating signals disperse with the wavevector. The colour map in Fig. 3a represents the absolute value of the Fourier transform of $\Delta I(t)/I_0$ for different wavevectors along the [001] direction. We observed two dispersive modes around 0.4 and 1 THz, which we assigned to the TA and TO branches, respectively[17,20,30]. The spectral intensity was strongest in the TA branch, which played a prominent role in the polar response reported in Fig. 2b,c. Figure 3b shows the dispersion relations at 20 K (blue) and 50 K (red) obtained from our measurements (Fig. 3a). The black dashed line shows the linear dispersion of the TA branch measured by Brillouin scattering[31] extrapolated to high wavevectors. The TO branch in Fig. 3b shows softening with decreasing temperature characteristic of the incipient FE[2,20]. Notably, the acoustic dispersion deviated from the extrapolated speed of sound at $\xi > 0.03$ rlu at 20 K, as can be seen in the zoomed-in trace of the TA branch in Fig. 3c. A similar anomaly has been observed by neutron scattering in equilibrium[17,20,30] and was associated with some form of coupling between the TO and TA branches. Compared with Fig. 3a, it is clear that $\xi > 0.03$ rlu is also where the TA branch had the strongest response to the pump and, hence, the strongest polar character. These results indicate that there was a common physical origin for the frequency softening of the acoustic modes and their strong polar character observed here.

Our measurements offer a deeper understanding of the interplay between strain ε and polarization P in $SrTiO_3$. In particular these results provide a robust characterization of their coupling and enabled us to build a new map of the precursor fluctuations of incipient orders, as presented in Fig. 4. $SrTiO_3$ is centrosymmetric, which imposes constraints on the possible interactions between P, which is odd upon inversion, and ε, which is even. The inversion of the TA signal with field polarity indicates that the coupling is odd with P and must, therefore, strictly involve gradients of ε to respect the centrosymmetry. To leading order, this interaction is the flexoelectric coupling[7,32–36], which is bilinear in P and ε, $\mathcal{O}(P\nabla\varepsilon)$ (ref. 21). The flexoelectricity vanishes near the zone centre ($\xi = 0$), where the leading coupling is electrostrictive and is quadratic in P (ref. 9), $\mathcal{O}(P^2\varepsilon)$. If electrostriction were the dominant interaction at the wavevectors k where we observe a dynamic signal, it would produce a non-inverting response and a quadratic dependence of the TA oscillation amplitude on the terahertz field strength. Instead, flexoelectricity explains our main observations: (1) the odd symmetry of both modes upon inversion, (2) the softening of the acoustic branch

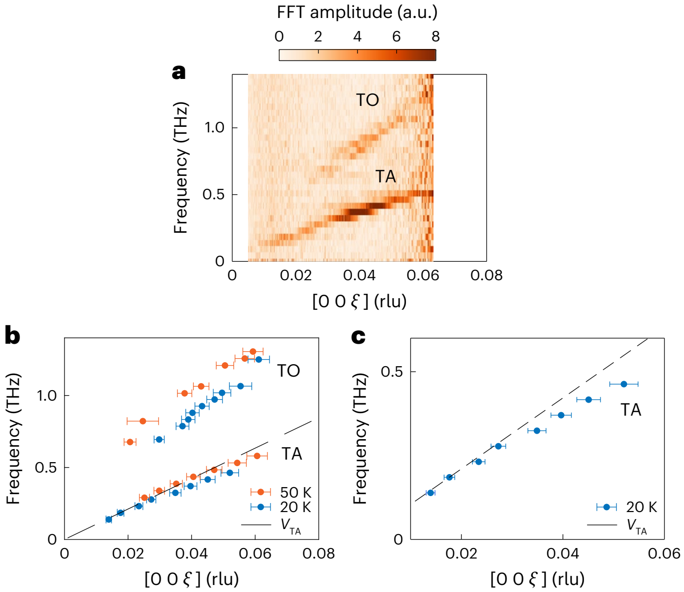

Fig. 3 | Dispersion relation of coherent excitations. a, Colour map representing the magnitude of the Fourier transform of time-domain data at a temperature $T = 20$ K, like those presented in Fig. 1c, for different wavevectors. **b**, Dispersion relation obtained by fitting the peak position for each frequency bin in **a**. The error bars represent the 95% confidence bounds of the fit, combined with the error from the estimated maximum possible misalignment of the crystal. The dashed line represents the speed of sound of TA modes from Brillouin scattering data[31]. **c**, Zoomed-in view of the TA branch dispersion relation at $T = 20$ K showing the deviation from the linear dispersion represented by the dashed line. FFT, fast Fourier transform.

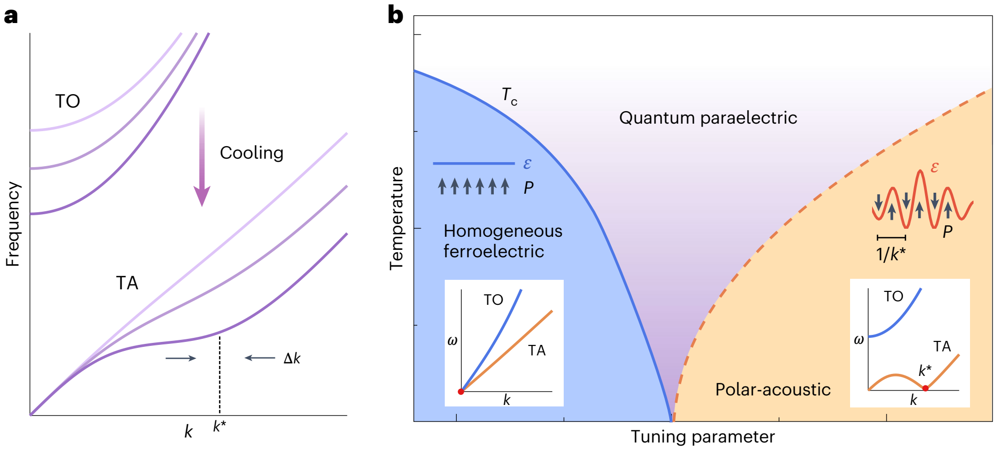

Fig. 4 | Lattice instability towards a modulated structure. a, Schematic illustration of the dispersion of transverse phonon modes. As the temperature decreases, the TO branch softens and the TA branch deviates from linear dispersion developing a kink at finite wavevector k^*, indicative of an instability. These excitations are polar and modulate the polarization spatially with a wavelength ~$2\pi/k^*$. **b**, Schematic phase diagram of SrTiO$_3$ showing the nearby phases around the quantum paraelectric regime. The blue and orange areas represent the FE phase and a polar-acoustic regime[19,21]. In the former, the polarization is homogeneous whereas in the latter, the strain and polarization are modulated spatially with period $2\pi/k^*$. The flexoelectric coupling strength could be taken as the tuning parameter. T_c is the FE Curie temperature. The left and right insets show illustrations of the dispersion relation similar to **a** close to the transitions to the FE phase and polar-acoustic regime, respectively.

at finite wavevectors and (3) the linearity of the TA oscillations with field strength (Supplementary Fig. 3). Importantly, a sufficiently large flexoelectric coupling gives rise to exotic modulated instabilities and phases[21].

We summarize these results qualitatively in Fig. 4a, which illustrates the dispersion relation at different temperatures taking into account the flexoelectric coupling[21,32,33]. The TO branch softens considerably at the zone centre upon cooling[37] and corresponds to the order parameter of the incipient FE phase. Simultaneously, coupling between the TO and TA branches causes the softening and deviation from linear dispersion of the TA branch around the wavevector k^* and an increase of its polar character.

Figure 4b is a schematic phase diagram of SrTiO$_3$ (refs. 16,18,19,21) as a function of temperature and the flexoelectric coefficient that governs the TO–TA coupling strength. The diagram illustrates that the quantum paraelectric regime separates a homogeneous FE phase, where the zone-centre TO mode softens to zero frequency ω, from a putative polar-acoustic regime[19], where the acoustic branch softens at k^* and strongly enhances the polarization and strain modulation at this wavevector. While the soft TO mode is a precursor of the spatially homogeneous FE phase (light blue region in Fig. 4b), the polar-acoustic modes observed here are the precursors of a possible modulated polar-acoustic phase (orange region in Fig. 4b)[19,21].

Our measurements have unveiled the local polar excitations in SrTiO$_3$, which shape its quantum critical behaviour and could foster unconventional superconductivity[38]. These polarization density waves, which arise from a flexoelectric interaction, provide direct evidence of a modulated polar instability in SrTiO$_3$, which may suppress its ferroelectricity[21]. More generally, nanoscale instabilities often herald exotic and sought-after phases in materials with complex phase diagrams. Our results show that time-resolved measurements with access to finite wavevectors can reveal new instabilities that are key to unlocking and controlling new phases of complex materials.

Online content

Any methods, additional references, Nature Portfolio reporting summaries, source data, extended data, supplementary information, acknowledgements, peer review information; details of author contributions and competing interests; and statements of data and code availability are available at https://doi.org/10.1038/s41567-025-02874-0.

References

1. Weaver, H. Dielectric properties of single crystals of SrTiO$_3$ at low temperatures. *J. Phys. Chem. Solids* **11**, 274–277 (1959).
2. Shirane, G. & Yamada, Y. Lattice-dynamical study of the 110°K phase transition in SrTiO$_3$. *Phys. Rev.* **177**, 858–863 (1969).
3. Müller, K. A. & Burkard, H. SrTiO$_3$: an intrinsic quantum paraelectric below 4 K. *Phys. Rev. B* **19**, 3593–3602 (1979).
4. Bussmann-Holder, A., Beige, H. & Völkel, G. Precursor effects, broken local symmetry, and coexistence of order-disorder and displacive dynamics in perovskite ferroelectrics. *Phys. Rev. B* **79**, 184111 (2009).
5. Bussmann-Holder, A. & Bishop, A. R. Intrinsic inhomogeneity as origin of incomplete ferroelectricity. *Europhys. Lett.* **76**, 945 (2006).
6. Laguta, V. V., Blinc, R., Itoh, M., Seliger, J. & Zalar, B. ^{87}Sr NMR of phase transitions in SrTi^{16}O$_3$ and SrTi^{18}O$_3$. *Phys. Rev. B* **72**, 214117 (2005).
7. Biancoli, A., Fancher, C. M., Jones, J. L. & Damjanovic, D. Breaking of macroscopic centric symmetry in paraelectric phases of ferroelectric materials and implications for flexoelectricity. *Nat. Mater.* **14**, 224–229 (2015).
8. Haeni, J. H. et al. Room-temperature ferroelectricity in strained SrTiO$_3$. *Nature* **430**, 758–761 (2004).
9. Xu, R. et al. Strain-induced room-temperature ferroelectricity in SrTiO$_3$ membranes. *Nat. Commun.* **11**, 3141 (2020).
10. Bednorz, J. G. & Müller, K. A. Sr$_{1-x}$Ca$_x$TiO$_3$: an XY quantum ferroelectric with transition to randomness. *Phys. Rev. Lett.* **52**, 2289–2292 (1984).
11. Itoh, M. et al. Ferroelectricity induced by oxygen isotope exchange in strontium titanate perovskite. *Phys. Rev. Lett.* **82**, 3540–3543 (1999).
12. Li, X. et al. Terahertz field-induced ferroelectricity in quantum paraelectric SrTiO$_3$. *Science* **364**, 1079–1082 (2019).
13. Nova, T. F., Disa, A. S., Fechner, M. & Cavalleri, A. Metastable ferroelectricity in optically strained SrTiO$_3$. *Science* **364**, 1075–1079 (2019).
14. Cheng, B., Kramer, P. L., Shen, Z.-X. & Hoffmann, M. C. Terahertz-driven local dipolar correlation in a quantum paraelectric. *Phys. Rev. Lett.* **130**, 126902 (2023).

15. Shin, D. et al. Simulating terahertz field-induced ferroelectricity in quantum paraelectric $SrTiO_3$. *Phys. Rev. Lett.* **129**, 167401 (2022).
16. Müller, U., Berlinger, W. & Tosatti, E. Indication for a novel phase in the quantum paraelectric regime of $SrTiO_3$. *Z. Phys. B* **84**, 277–283 (1991).
17. Vacher, R. et al. Anomalies in the TA-phonon branches of $SrTiO_3$ in the quantum paraelectric regime. *Europhys. Lett.* **17**, 45–49 (1992).
18. Rowley, S. E. et al. Ferroelectric quantum criticality. *Nat. Phys.* **10**, 367–372 (2014).
19. Coak, M. J. et al. Quantum critical phenomena in a compressible displacive ferroelectric. *Proc. Natl Acad. Sci. USA* **117**, 12707–12712 (2020).
20. Fauqué, B. et al. Mesoscopic fluctuating domains in strontium titanate. *Phys. Rev. B* **106**, L140301 (2022).
21. Guzmán-Verri, G. G., Liang, C. H. & Littlewood, P. B. Lamellar fluctuations melt ferroelectricity. *Phys. Rev. Lett.* **131**, 046801 (2023).
22. Trigo, M. et al. Fourier-transform inelastic X-ray scattering from time- and momentum-dependent phonon–phonon correlations. *Nat. Phys.* **9**, 790–794 (2013).
23. Emma, P. et al. First lasing and operation of an ångstrom-wavelength free-electron laser. *Nat. Photonics* **4**, 641–647 (2010).
24. Kozina, M. et al. Terahertz-driven phonon upconversion in $SrTiO_3$. *Nat. Phys.* **15**, 387–392 (2019).
25. Kubacka, T. et al. Large-amplitude spin dynamics driven by a THz pulse in resonance with an electromagnon. *Science* **343**, 1333–1336 (2014).
26. Lytle, F. W. X-ray diffractometry of low-temperature phase transformations in strontium titanate. *J. Appl. Phys.* **35**, 2212–2215 (1964).
27. Hayward, S. A. & Salje, E. K. H. Cubic-tetragonal phase transition in $SrTiO_3$ revisited: Landau theory and transition mechanism. *Phase Transitions* **68**, 501–522 (1999).
28. Aschauer, U. & Spaldin, N. A. Competition and cooperation between antiferrodistortive and ferroelectric instabilities in the model perovskite $SrTiO_3$. *J. Phys.: Condens. Matter* **26**, 122203 (2014).
29. Yamanaka, A. et al. Evidence for competing orderings in strontium titanate from hyper-Raman scattering spectroscopy. *Europhys. Lett.* **50**, 688 (2000).
30. Stirling, W. G. Neutron inelastic scattering study of the lattice dynamics of strontium titanate: harmonic models. *J. Phys. C* **5**, 2711–2730 (1972).
31. Hehlen, B., Kallassy, Z. & Courtens, E. The high-frequency elastic constants of $SrTiO_3$ in the quantum paraelectric regime. *Ferroelectrics* **183**, 265–272 (1996).
32. Tagantsev, A. K. & Yudin, P. V. (eds) *Flexoelectricity in Solids: From Theory to Applications* (World Scientific, 2016).
33. Zubko, P., Catalan, G. & Tagantsev, A. K. Flexoelectric effect in solids. *Annu. Rev. Mater. Res.* **43**, 387–421 (2013).
34. Yudin, P. V. & Tagantsev, A. K. Fundamentals of flexoelectricity in solids. *Nanotechnology* **24**, 432001 (2013).
35. Wang, B., Gu, Y., Zhang, S. & Chen, L.-Q. Flexoelectricity in solids: progress, challenges, and perspectives. *Prog. Mater. Sci.* **106**, 100570 (2019).
36. Zubko, P., Catalan, G., Buckley, A., Welche, P. R. L. & Scott, J. F. Strain-gradient-induced polarization in $SrTiO_3$ single crystals. *Phys. Rev. Lett.* **99**, 167601 (2007).
37. Yamada, Y. & Shirane, G. Neutron scattering and nature of the soft optical phonon in $SrTiO_3$. *J. Phys. Soc. Jpn* **26**, 396–403 (1969).
38. Hameed, S. et al. Enhanced superconductivity and ferroelectric quantum criticality in plastically deformed strontium titanate. *Nat. Mater.* **21**, 54–61 (2022).
39. Naftaly, M. & Miles, R. A method for removing etalon oscillations from THz time-domain spectra. *Opt. Commun.* **280**, 291–295 (2007).

Methods

Experimental details

Single-crystal $SrTiO_3$ was commercially obtained from MTI Corp and was like the sample used in ref. 12. The 10 × 10 × 0.5-mm^3 sample was Verneuil-grown, with two sided epi-polished (001) surfaces. Measurements were taken at sample temperatures of 20 and 50 K in the cryogenic-compatible vacuum chamber at the X-ray pump–probe end station at the Linac Coherent Light Source[40]. The sample was mounted inside a vacuum-compatible chamber with translation and rotation motions required to reach the desired X-ray diffraction and scattering conditions. A dedicated copper mount was fabricated for this purpose. The mount allowed us to pre-tilt the sample by 10° so that we could reach the (3, 3, 3) diffraction peak at 10.4 keV and measure the scattering around it. The crystal was cooled by a helium flow cryostat. The cold finger was connected with flexible copper braids to the dedicated mount, and the temperature was measured by a diode fixed close to the sample position.

Intense terahertz fields were generated by optical rectification of 120 fs, near-IR (NIR) pulses centred at 800 nm in $LiNbO_3$ using the tilted-pulse-front technique[41–44]. To generate terahertz fields with inverted polarities, two $LiNbO_3$ prisms were mounted vertically one on top of the other outside the vacuum chamber and with their FE polarizations pointing in opposite directions. A motorized vertical translation stage was used to switch between the prisms in the 800-nm beam path. The temporal profile of the two inverted fields at the sample position was measured using electro-optic sampling in a 100-μm GaP crystal (Fig. 2a). The intensity and polarization of the terahertz pulses were controlled by a pair of wire-grid polarizers. An off-axis parabolic mirror inside the chamber with a focal length of 76.2 mm was used to focus the pulses into an ~1-mm-diameter spot on the sample position. The beam profile was characterized with an Ophir Pyrocam IIIHR.

The lattice dynamics was probed by diffraction and scattering of 50-fs, 10.4-keV hard X-ray pulses focused to a 300-μm-diameter spot. A small hole in the terahertz focusing mirror was used for transporting the X-rays and allowed collinear propagation of the X-ray and terahertz pulses, which impinged on the sample at an angle of ~30°. The scattered photons were recorded through a Kapton window by a Jungfrau area detector positioned outside the chamber and 300 mm from the sample. To match the pumped and probed volumes while maximizing the pump fluence, we implemented a grazing exit geometry. The exit angle was set to ~1° with respect to the sample surface such that the detected X-ray photons originated from a region <1 μm into the sample, comparable to the penetration depth of the terahertz pulse in $SrTiO_3$ at low temperatures. No appreciable heating from the terahertz excitation was observed during the experiment (Supplementary Fig. 4).

Data availability

The datasets generated and analysed during the current study are available from the corresponding author on reasonable request.

References

40. Chollet, M. et al. The X-ray pump–probe instrument at the Linac Coherent Light Source. *J. Synchrotron Radiat.* **22**, 503–507 (2015).
41. Hebling, J., Yeh, K.-L., Hoffmann, M. C., Bartal, B. & Nelson, K. A. Generation of high-power terahertz pulses by tilted-pulse-front excitation and their application possibilities. *J. Opt. Soc. Am. B* **25**, B6 (2008).
42. Fülöp, J. A., Pálfalvi, L., Hoffmann, M. C. & Hebling, J. Towards generation of mJ-level ultrashort THz pulses by optical rectification. *Opt. Express* **19**, 15090 (2011).
43. Yeh, K.-L., Hoffmann, M. C., Hebling, J. & Nelson, K. A. Generation of 10 μJ ultrashort terahertz pulses by optical rectification. *Appl. Phys. Lett.* **90**, 171121 (2007).
44. Hoffmann, M. C. & Fülöp, J. A. Intense ultrashort terahertz pulses: generation and applications. *J. Phys. D* **44**, 083001 (2011).

Acknowledgements

We acknowledge insightful discussions with B. Fauqué, G. Guzmán-Verri and P. Littlewood. The experimental work was supported by the US Department of Energy, Office of Science, Office of Basic Energy Sciences through the Division of Materials Sciences and Engineering (Contract Nos. DE-AC02-76SF00515 with G.O., V.K., Y.H., G.d.l.P.M., R.A.D., D.R. and M.T. and DE-SC0019126 with Z.Z., R.C. and K.A.N.). Work at Brookhaven is supported by the Office of Basic Energy Sciences, Materials Sciences and Engineering Division, US Department of Energy (Contract No. DE-SC0012704). Use of the Linac Coherent Light Source was supported by the US Department of Energy, Office of Science, Office of Basic Energy Sciences (Contract No. DE-AC02-76SF00515). S.L.J. acknowledges support from the Swiss National Science Foundation (Project Grant No. 200020_192337). Work at Harvard University was supported by the US Department of Energy, Office of Basic Energy Sciences, Early Career Award Program (Award No. DE-SC0022883). J.S. acknowledges support from the NSF (REU Supplement No. 2133686 under Award No. 2019014).

Author contributions

M.T. and K.A.N. conceived the study. G.O., V.K., Y.H., Z.Z., G.d.l.P.M., R.A.D., Q.N., J.S., S.T., H.Y., T.S., M.C.H., P.K., A.C., R.C., M.P.M.D., A.S.D., M.F., S.L.J., M.M., D.R., D.Z., K.A.N. and M.T. performed the experiment. G.O. and V.K. analysed the data. G.O., V.K., J.Z. A.S.D, A.M.R., K.A.N. and M.T. interpreted the data. G.O., V.K. and M.T. wrote the paper with contributions from all authors.

Competing interests

The authors declare no competing interests.

Additional information

Supplementary information The online version contains supplementary material available at https://doi.org/10.1038/s41567-025-02874-0.

Correspondence and requests for materials should be addressed to Mariano Trigo.

Peer review information *Nature Physics* thanks the anonymous reviewers for their contribution to the peer review of this work.